FLEXIBILITY OF AN ORNITHOPTER WING TESTED IN A WIND TUNNEL

M. B. Jones A. Valiyff , J. Harvey

Air Vehicles Division, Defence Science and Technology Organisation, Fishermans Bend, VIC, 3207 Australia, (03)9626 7039, malcolm.jones@dsto.defence.gov.au, aliya.valiyff@dsto.defence.gov.au, james.harvey@dsto.defence.gov.au

Keywords: *Ornithopter, flapping, wing deformation*

Abstract

Using high speed video tracking, the surface topography of an ornithopter wing is quantified for a range of flapping frequencies and free stream velocities. Based on Fourier series fits, relatively simple analytical models of the surface topography are determined for a complete flapping cycle.

1   Introduction

For natural flyers, large deformations of the wing surface have been observed. The inertial loads generated by a flapping wing require that the wing mass is kept to a minimum, as a consequence, engineered flapping wings will also be inherently flexible. In addition, there is evidence which suggests that for flapping flight, flexibility plays an important role in the generation of lift and thrust [1–4]. Therefore, methods for predicting the performance of flapping wings must treat the aerodynamics, the inertia and the structural response of the wing as well as the complex interplay between the two phenomena.

In order to further understand the fluid structural interactions, simultaneous measurements have been made of the (i) time resolved forces and moments acting on the wing (ii) time resolved pressures acting on the wing and (iii) the wing kinematics and deformations. In this paper we focus only on the wing kinematics and deformations; and present the experimental technique used, analysis methods and typical results.

2   Experimental Method

2.1   Ornithopter model

Videogrammetry was undertaken for a commercially purchased ornithopter with half span of 0.325 m. Flapping motion was generated by a rotating crank mechanism driven by a brushless electric motor, creating a maximum flapping rate of $f \approx 9$ Hz and peak to peak amplitude of 52° [5], where f is the flapping frequency.

The leading edge (LE) strut is a carbon fibre rod and performs a nominal sinusiodal variation of its dihedral angle. The skin of the wing is made of rip-stop nylon supported with carbon fibre battens that are taped to the surface of the cloth in order to increase the stiffness of the wing, Figure 1. The leading edge of the nylon cloth has a sleeve which contains the LE strut. The sleeve is a "loose fit" and this allows the nylon cloth to rotate freely (i.e. twist) about the carbon fibre rod.

2.2   Wind tunnel and test matrix

The tests were performed in a closed-circuit, low speed wind tunnel, with a test section of 2.7-m wide and 2.1-m high. Table 1 summarises the test matrix used.

2.3   Motion Capture

The deformation of the port wing of the ornithopter was captured using a Vicon MX mo-

Fig. 1 Wing structure.

	U (m/s)								
	0	2	4	5	6	7	8	9	10
f (Hz)									
2	×	×	×	×	×	×	×	×	×
3	×	×	×	×	×	×	×	×	
4	×	×	×	×	×	×	×	×	×
5	×	×	×	×	×	×	×	×	
6	×	×	×	×	×	×	×	×	
7	×	×	×	×	×	×	×	×	

Table 1 Nominal freestream velocities and flapping frequencies.
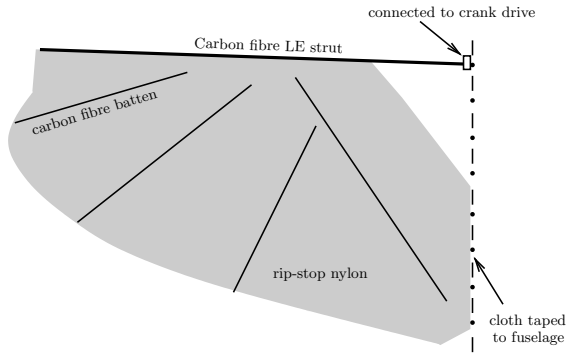
tion capture system. The system uses multiple cameras to capture the 3-dimensional motion of reflective markers which are illuminated in the infrared (IR) band.

A total of 36 reflective markers were placed on the upper surface of the wing, Figure 2. Three reference markers were also placed along the fuselage. The markers were circular having a diameter of 3 mm and a thickness of approximately 0.1 mm. Relative to the wing mass, the added mass of the markers was judged to be insignificant. Similarly the flow disturbance of the markers was small relative to the gross movements and deflections of the wing during flapping.
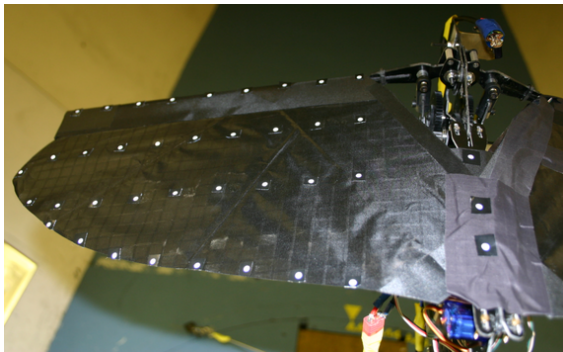
Fig. 2 Location of retro-reflective markers

Six Vicon MX-13 digital cameras operated at 500 frames per second (fps) were used to capture the motion of the port wing of the ornithopter. The MX-13 cameras incorporate an array of IR light emitting diodes (LEDs) placed circumferential around the camera lens. The LEDs provide the light source to the reflective markers and IR filters are fitted to the cameras to attenuate un-

wanted light sources illuminating the sensor. The cameras perform real-time processing of the sensor image and stream data representing the position and radius of each marker. The data is streamed to a single MX Ultranet control box which provides the power source, communication and synchronization of the camera data. The MX Ultranet controller communicates with the host PC running Vicon-Nexus software. Using the Nexus software, the 3-dimensional trajectories of each marker can be determined as a function of time.

3 Wing surface model

Due to the coupling between the aerodynamic and structural fields, mathematical models of the structure that describes the deformations in terms of aerodynamically relevant parameters are required. These parameters are dynamic functions of time and are referred to as the "wing parameters". The wing parameters may include: camber, wing twist, sectional angle-of-attack etc.

Due to the cyclic nature of the motion, a Fourier series based approach is taken, whereby, the relevant wing parameters are described in terms of truncated Fourier series functions. Such a model provides a framework for quantifying and specifying the structural response of the wing in the most concise form. The Fourier series approach also allows the fidelity of the model to be tuned by simply adding further terms to the series.

The motion of the wing surface can be decomposed into two parts, wing root kinematics caused by the flapping mechanism and dynamic wing deflections driven by both aerodynamic and

inertial loads. The wing has a single degree of rotational freedom and the motion can be defined by the dihedral angle of the LE strut, measured at the wing root; this will be referred to as the flap angle ϕ. Superimposed on the wing root kinematics are the surface deflections and these are decomposed further into: (i) spanwise bending of the LE strut, (ii) spanwise twisting of wing sections about the LE strut and (iii) camber of the wing sections. However, when analysing the sectional profiles it was found that the amount of induced camber is negligible in comparison to the bending and twisting modes.

The aim of the work is then to determine analytical functions that can be used to specify the wing topography at any instant in time.

4   Results

For the purpose of analysis $t = 0$ is defined to occur at the bottom of the stroke. The cycle period is denoted by $T = 1/f$. Generally 2 to 3 seconds of data was captured for a fixed test point. This yielded 5 to 20 cycles of data at a given test point. The data was reduced to a single cycle representation by phase averaging over the total number of complete cycles. This has the effect of removing any noise in the data. However, it was found the the difference between the phase averaged data and a single cycle of data was small, indicating that the flapping cycle is repeatable and that the data has a high signal to noise ratio.

Two coordinate systems are defined, an inertial reference frame, fixed in space (X-Y-Z) and a non-inertial, rotating reference frame (x-y-z), Figure 3. The X axis is parallel to the fuselage, the Y axis is normal to the fuselage, directed spanwise in the port direction and Z is downwards normal to the fuselage. The flapping angle, ϕ, is defined as the dihedral angle of the wing and this angle varies during a flapping cycle. The x-y-z sytem is related to the X-Y-Z system by a rotational transformation of ϕ about the X-axis. The origin of both the coordinate systems is located at the point of rotaion of the leading edge strut.

In the analysis that follows, the Fourier series
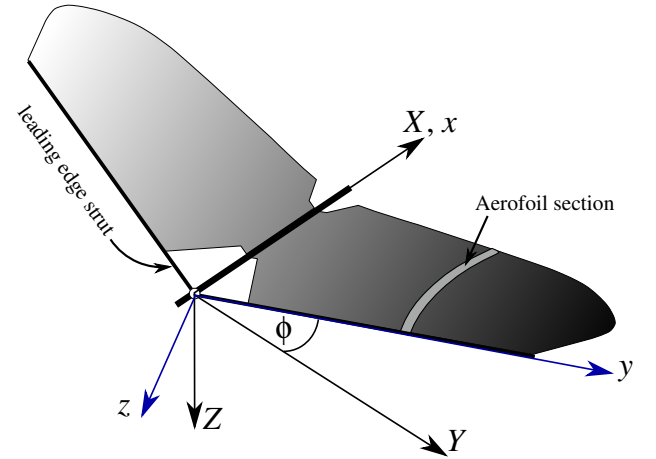
Fig. 3 Definition of coordinate systems.

defined by

$$p(t) = a_0 + \sum_{n=1}^{\infty} \left(a_n \cos nt' + b_n \sin nt' \right) \quad (1)$$

will be used to model some wing parameter, $p(t)$, where $t' = -\pi + 2\pi ft$, a_0, a_n and b_n are the Fourier series coefficients where n is an integer.
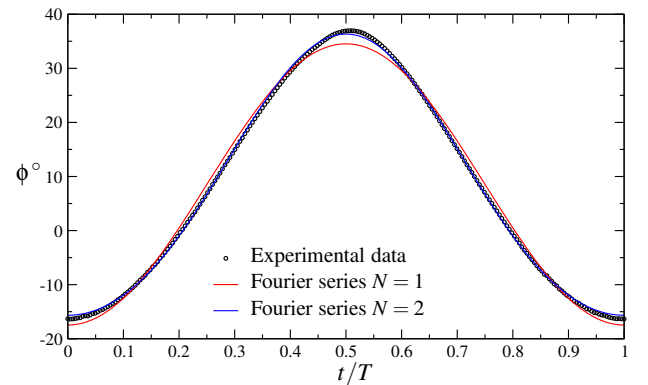
Fig. 4 Flap angle (ϕ) as measured by the most inboard marker on the leading edge strut.

4.1   Wing kinematics

The wing root kinematics were determined by tracking a marker placed on the leading edge and a distance of approximately 65 mm from the axis of rotation. For a flapping frequency of $\sim 2\,\mathrm{Hz}$ the trajectory of this marker can be taken to be due to the wing root kinematics alone. Figure 4 shows the flapping angle, ϕ, over a cycle as measured by this marker for the case of $f \sim 2\,\mathrm{Hz}$ and

$U = 0$ m/s. The data of Figure 4 is compared to Fourier cosine series fits with $N = 1$ and $N = 2$, where N is the number of Fourier cosine coefficients. The kinematics are found to deviate from pure cosine flapping ($N = 1$). However increasing the number of coefficients to $N = 2$ results in a good fit to data, where the Fourier cosine coefficients are found to be $a_0 = 8.54$, $a_1 = 26.0$ and $a_2 = 1.81$. Note, $b_n = 0$ for all n.
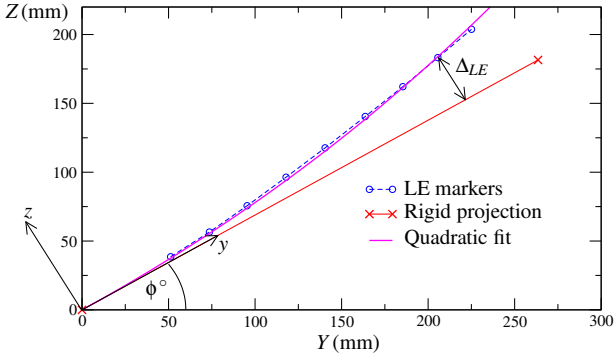
Fig. 5 Deflection of LE strut at top of stroke, compared to rigid kinematics and quadratic curve fit. Data from test point $U = 0$ m/s and $f = 7$ Hz.

4.2 Leading edge bending

During flapping, bending of the leading edge strut occurs. Figure 5 shows the the Y-Z coordinates of markers placed on the leading edge strut at the top of the stroke, for the case of $f = 7$ Hz and $U = 0$. For comparison, a rigid projection of the wing root kinematics (equivalent to y-axis) is also shown in Figure 5 and the difference between these two curves is defined by Δ_{LE}. A quadratic function of the form

$$\Delta_{LE} = \frac{y^2}{2R} \qquad (2)$$

was fitted to the difference and the fit is also shown in Figure 5. The curve fit (2) was used to approximate the curvature (κ in m^{-1}) of the leading edge strut, for each instant in time. Given, that for the data, $y/R \ll 1$, it can be shown that $\kappa \approx$ constant $= 1/R$, for a given instant in time. Following this method, the values of κ were determined during a cycle and an example is plotted

in Figure 6. A Fourier series with $N = 2$ provides a good model for the LE curvature variation as a function of time, also shown in Figure 6. The total number of paramters required to specify the bending is 5.
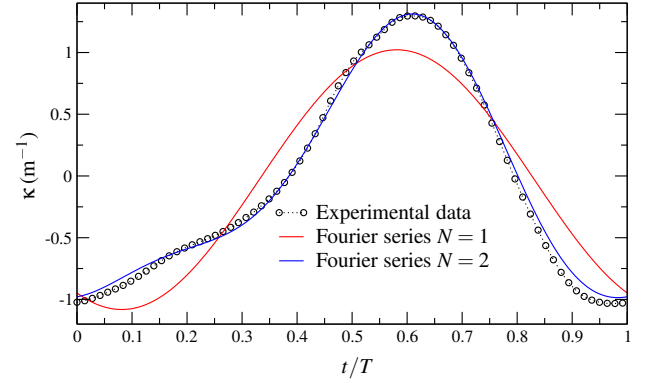
Fig. 6 Curvature, κ, of the leading edge as a function of time. Data from test point $U = 0$ m/s and $f = 7$ Hz.

4.3 Spanwise twist

Due to aerodynamic and inertial loads the pitch angle (θ) of a given wing section varies over a flap cycle. The pitch angle is defined as the angle of rotation of an aerofoil section (Fig. 3) about the LE strut (y-axis). For example when $\theta = 0$ the aerofoil section lies in the x-y plane whereas for a positive value of θ the trailing edge of the section sits below the x-y plane. The value of θ was determined based on the angle between the x-y plane and the straight line joining the marker on the LE to the marker on the TE. Figure 7 shows the variation of pitch angle with time for the aerofoil section located at $y/b = 0.7$ ($b = 325$ mm is the semi-span of the wing), for the case of $f = 7$ Hz and $U = 0$. For comparison Fourier representations of the data using $N = 2$ and $N = 3$ are shown.

Figure 8 shows the Fourier series fits ($N = 3$) for the all spanwise station for the case of $f = 7$ Hz and $U = 0$. The variation of pitch angle with time for all the spanwise stations is similar and there is a linear increase in the peak-peak amplitue of the twist with the spanwise coordinate y. The self-similarity of the profiles in Figure 8
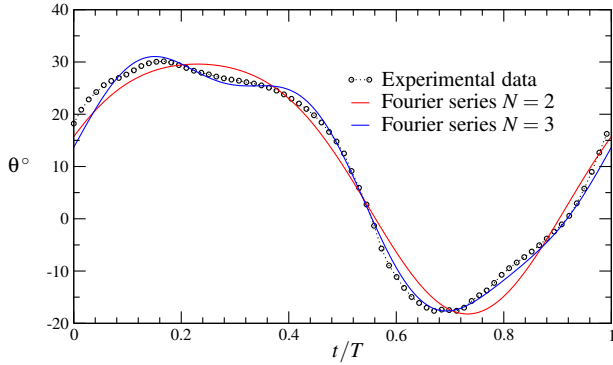
Fig. 7 Pitch angle variation measured at a section located approximated 2/3 of the semi-span from the wing root.

allows the twist function to be specified by a single Fourier series, for a given combination of U and f. The Fourier series fit is then scaled by the local y-coordinate, such that

$$\theta(y,t) = y\,p(t) \qquad (3)$$

where $p(t)$ is the Fourier series. The twist peak-peak amplitude is found to increase with flapping frequency but decrease with freestream velocity, as shown in Figure 9.
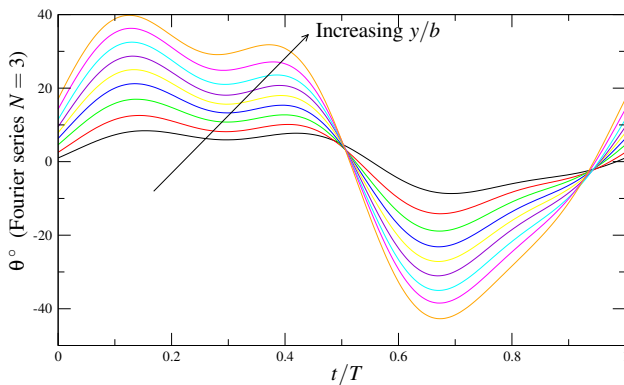
Fig. 8 Fourier series fits to pitch angle variation for all the spanwise stations.

4.4 Camber

The structure of the wing is described in section 2.1 and the wing surface is essentially a thin flat plate when not loaded. Under the combined aerodynamic and inertia loads the aerofoil sections deviate from a constant thickness flat plate,
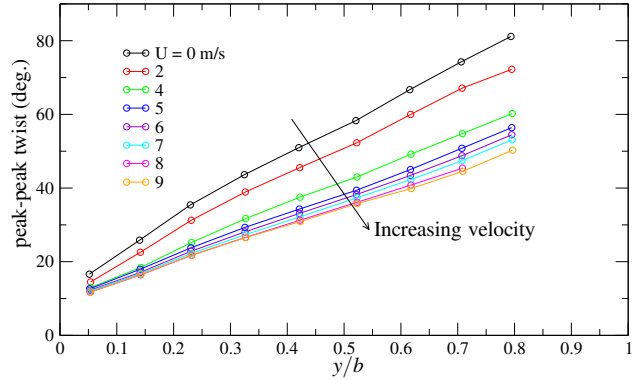
Fig. 9 Peak-peak twist amplitude as a function of y/b for varying U.

to a constant thickness cambered aerofoil. Generally the amount of induced camber was negligible. However, for the case of $f = 7\,\text{Hz}$ combined with a freestream velocity of $U = 8\,\text{m/s}$, a reflex camber was observed to develop on the 5 outboard stations ($y/b > 0.6$). This reflexed camber was dominanted by a "folding" of the trailing edge and may be associated with a flutter type instability. Typical results for this particular case are given in Figure 10 for an outboard station, at four instants in time ($t/T = 0, 1/4, 1/2, 3/4$).

As the measured camber was negligible in all instances, except for the $f = 7\,\text{Hz}$, $U = 8\,\text{m/s}$ case, it will not be included in the general mathematical model that describes the wing deformation.
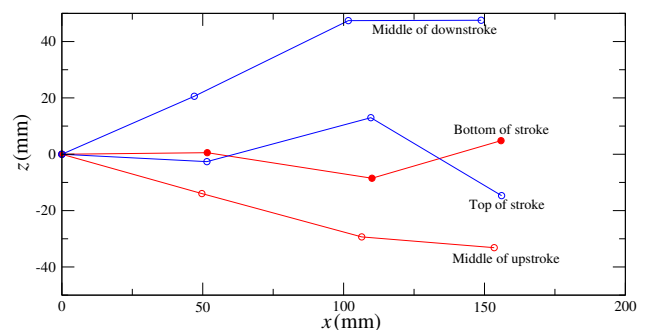
Fig. 10 Aerofoil sections for outboard station ($y/b = 0.7$), showning combined effect of pitch and camber. Shown at four instant in time.

4.5 Mathematical model of wing surface

Using the functional fits determined above, the surface can be fully described as a function of time over a cycle. For a given point on the wing its trajectory in the *x-y-z* frame can be approximately modelled using

$$x = x' \cos[\theta(y',t)] \tag{4}$$
$$y = y' \tag{5}$$
$$z = \Delta_{LE}(y',t) + x' \sin[\theta(y',t)] \tag{6}$$

where (x',y') is the location of the point on a static wing and with $U = 0$. There are a total of 12 parameters required to specify equations (4)-(6). Using a coordinate transformation the point on the wing in the inertial reference frame is then given by

$$\begin{bmatrix} X \\ Y \\ Z \end{bmatrix} = \begin{bmatrix} 1 & 0 & 0 \\ 0 & \cos\phi & -\sin\phi \\ 0 & \sin\phi & \cos\phi \end{bmatrix} \begin{bmatrix} x \\ y \\ z \end{bmatrix} \tag{7}$$

Representations of the wing surface using equations (4)-(7) are shown in Figure 11 for four instants in time, for the case of $f = 7\,\text{Hz}$ and $U = 0$.

5 Conclusions

The kinematics and wing deflections of an ornithopter tested in a windtunnel have been captured using high speed videogrammetry. Using Fourier series analysis the data can be reduced to analytical functions that describe the wing topography at any instant in time. The analytical representations provide a concise way to represent the data for input into aerodynamic models and CFD fluid structural interaction development. The Fourier analysis also provides a framework to compare and correlate the force, moment and pressure data which was simultaneously acquired in the experiments.

References

[1] A Agrawal and S.K Agrawal. Design of bio-inspired flexible wings for flapping-wing micro-sized air vehicle applications. *Advanced Robotics*, 23:979–1002, 2009.

[2] K.B. Lua, K.C. Lai, T.T. Lim, and K.S. Yeo. On the aerodynamic characteristics of hovering rigid and flexible hawkmoth-like wings. *Experiments in Fluids*, 49(6):1263–1291, 2010.

[3] W. Shyy, H. Aono, S.K. Chimakurthi, P. Trizila, C.-K. Kang, C.E.S. Cesnik, and H. Liu. Recent progress in flapping wing aerodynamics and aeroelasticity. *Progress in Aerospace Sciences*, 2010.

[4] R. J. Wootton. Function, homology and terminology in insect wings. *Systematic Entomology*, 4(1):81–93, 1979.

[5] Sean Kinkade. Hobbytechnik is flapping flight!, July 2010. URL http://www.flappingflight.com.

5.1 Copyright Statement
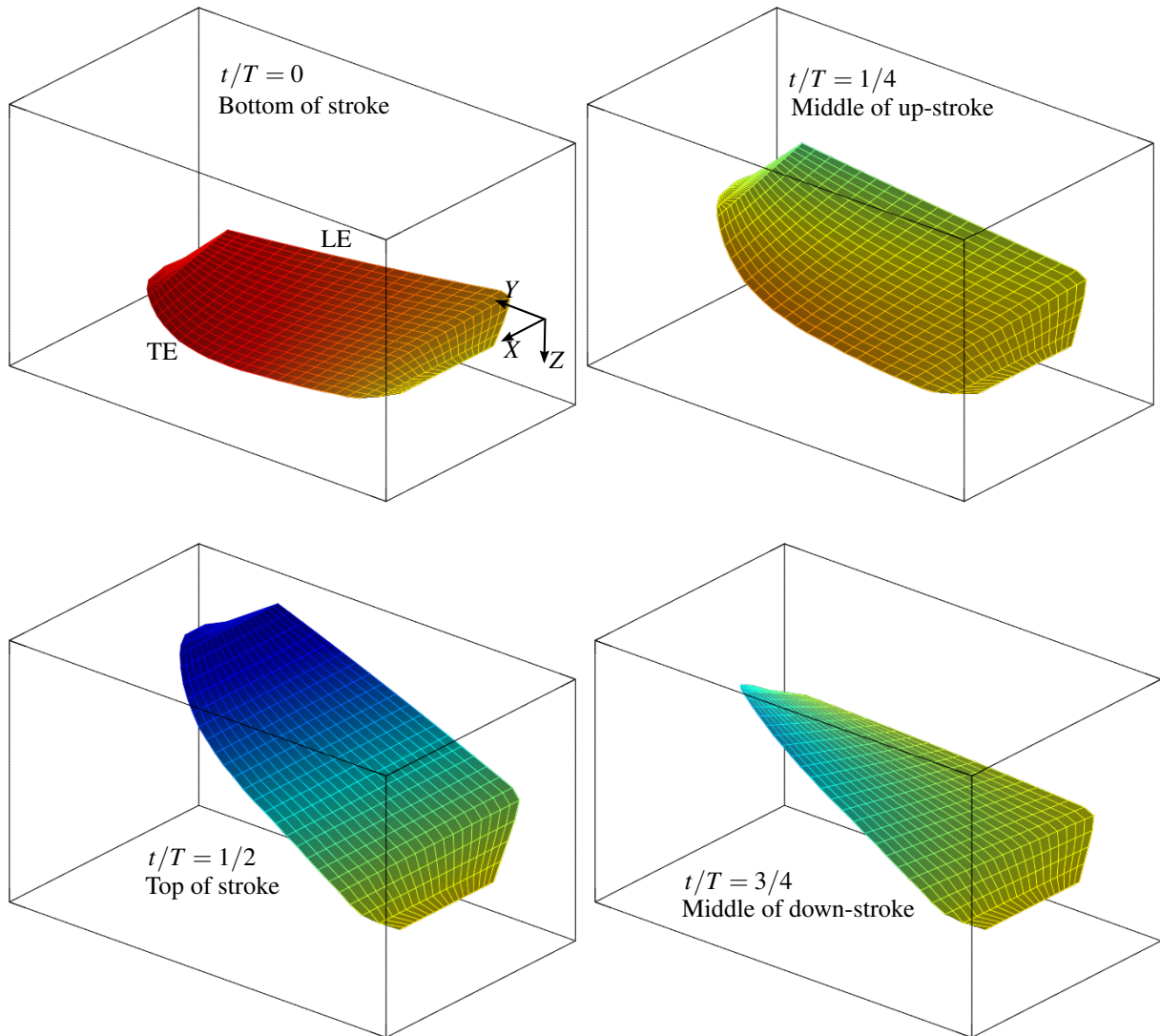
Fig. 11 Reconstruction of wing surface for the case of $f = 7\,\mathrm{Hz}$ and $U = 0$. Wing is shown at four instant in time.